REVIEW

Emerging methods for prostate cancer imaging: evaluating cancer structure and metabolic alterations more clearly

Adam Retter, Fiona Gong, Tom Syer, Saurabh Singh, Sola Adeleke and Shonit Punwani (iD)

UCL Centre for Medical Imaging, London, UK

Imaging plays a fundamental role in all aspects of the cancer management pathway. However, conventional imaging techniques are largely reliant on morphological and size descriptors that have well-known limitations, particularly when considering targeted-therapy response monitoring. Thus, new imaging methods have been developed to characterise cancer and are now routinely implemented, such as diffusion-weighted imaging, dynamic contrast enhancement, positron emission technology (PET) and magnetic resonance spectroscopy. However, despite the improvement these techniques have enabled, limitations still remain. Novel imaging methods are now emerging, intent on further interrogating cancers. These techniques are at different stages of maturity along the biomarker pathway and aim to further evaluate the cancer microstructure (vascular, extracellular and restricted diffusion for cytometry in tumours) magnetic resonance imaging (MRI), luminal water fraction imaging] as well as the metabolic alterations associated with cancers (novel PET tracers, hyperpolarised MRI). Finally, the use of machine learning has shown powerful potential applications. By using prostate cancer as an exemplar, this Review aims to showcase these potentially potent imaging techniques and what stage we are at in their application to conventional clinical practice.

1. Introduction

Imaging is implemented at every stage of the cancer management pathway, from diagnosis, staging, prognostication, surveillance and assessment of treatment response, to detection of complications following treatments and confirming remission [1]. The major advantage of imaging over other diagnostic tests remains its inherent ability to spatially localise disease.

Conventional imaging techniques – radiography, ultrasound (US), computerised tomography (CT) and magnetic resonance imaging (MRI) – rely upon morphological/anatomical features or descriptors in the evaluation of tumours. Features that are described qualitatively and subjectively, such as 'spiculated', 'moderate heterogeneity' and 'obscured margins', can help differentiate benign from malignant pathologies. However, although descriptors can provide an indicator towards malignancy, they are not perfect. For example, size is commonly employed as a classifier of malignancy within lymph nodes; yet, nodes less than a given size threshold may still harbour cancer (indicating limitations of sensitivity) [2,3], and those larger than the threshold may be enlarged due to alternative aetiology such as infection (indicating limitations of specificity) [4].

Abbreviations

ADC, apparent diffusion coefficient; CAD, computer-aided diagnosis; CT, computerised tomography; DCE, dynamic contrast enhancement; DL, deep learning; FDG, fludeoxyglucose (^{18}F); LWF, luminal water fraction imaging; ML, machine learning; Mp-MRI, multiparametric magnetic resonance imaging; PCa, prostate cancer; PET MRI, positron emission technology MRI; VERDICT, vascular, extracellular and restricted diffusion for cytometry in tumours.

Nonetheless, assessment of response to systemic cancer therapy remains contingent on size change, evaluated by response evaluation for solid tumours (RECIST) criteria, updated in 2009 to version 1.1 [5]. This has its limitations; for example, irregular and diffusely infiltrating lesions and lesions that are nonspherical are difficult to consistently measure, and diffuse bone lesions cannot be assessed altogether. Moreover, chemotherapeutic response may not itself cause a change in size and may, in some cases, increase the size of lesions [6]. Concealed responses can also occur, where imaging indicates no alteration in size when, histologically, there has been a complete response [7].

Significant effort is therefore focused on developing new imaging methods that can address these limitations. These methods aim to complement morphological imaging, with assessments of microstructure, function and metabolism – tissue attributes that are commonly altered in the development of cancer.

Within this Review, by using prostate cancer (PCa) MRI-based imaging as an exemplar, we highlight clinically available cancer imaging methods and showcase novel and emerging imaging methods which use our current clinical imaging infrastructure. Limiting the scope to PCa MRI enables detailed insight that may be transferrable to other cancers. PCa showcases a cancer where investigation with MRI is an extensively studied area, and it exhibits how the integration of researched functional imaging techniques can change the standard of care [8].

2. Current role of multiparametric MRI in prostate cancer

The traditional diagnostic pathway was based on a transrectal US-guided (TRUS) biopsy being offered to all men deemed at risk for PCa. However, high rates of overdiagnosis, missed significant lesions, misclassifications and potentially significant complications have led to the present implementation of multiparametric MRI (Mp-MRI) [9–13]. UK National Institute for Health and Care Excellent guidelines, updated on 09/05/2019, recommend that Mp-MRI be offered as the first-line investigation technique to people with suspected localised PCa [14]. Furthermore, the European Association of Urology strongly recommend that Mp-MRI be used before biopsies in biopsy-naïve men and, when MRIs are positive in this cohort [prostate imaging reporting and data system (PIRADS) ≥ 3], that targeted and systemic biopsies are performed, referring to the 'MRI pathway'.

Multiparametric-MRI combines anatomical sequences (T1- and T2-weighted MRI) and at least two functional

techniques that are readily clinically available. The added value of these techniques, as evidenced by the Prostate MRI Imaging Study trial, improves the detection of clinically significant disease compared with TRUS biopsies using transperineal template mapping biopsies as the reference standard (sensitivity of 93% vs 48%, negative predictive values 89% vs 74% in individuals with a Gleason score ≥ 4 + 3) [15]. The prospective multicentre PRECISION trial randomly assigned biopsy-naïve men to either have an Mp-MRI and a targeted biopsy (only if the MRI was positive) or a TRUS biopsy, without an Mp-MRI. In the Mp-MRI group, 28% of men avoided biopsy following a negative MRI and 38% of men that did receive targeted biopsies were diagnosed with clinically significant disease. Comparatively, 26% of men in the TRUS biopsy group were diagnosed with significant disease and more men were diagnosed with insignificant cancers (22% vs 9%) [16]. Similarly, the 4M study showed no difference in significant disease detection between the MRI and TRUS pathways (25% vs 23%); however, performing an MRI avoided biopsies in 49% of the men [17]. However, as shown by the multicentre MRI-FIRST study, in which patients received both TRUS biopsy and targeted biopsy if they were MRI positive, clinically significant PCa would have been missed in 5.2% of patients had a TRUS biopsy not been performed; thus, the need for TRUS biopsy was not excluded [18].

The functional imaging techniques utilised in the Mp-MRI pathway can achieve fewer men having biopsies, more significant disease identified and less overdetection of insignificant cancer. Despite the step change in diagnostic performance that Mp-MRI enables, it is not a perfect test. Significant research efforts focusing on the development of imaging to facilitate simplification, improve diagnostic accuracy and offer potential prognostic application are ongoing.

3. Clinically available functional imaging

Developing imaging methods follows a translational pipeline. Many methods emerge and are showcased in preclinical studies [19,20], however, only a few transition to first-in-human proof-of-concept studies [21]. These reports generate considerable excitement but seldom address repeatability, and the technique often remains immature, in that it does not have proven clinical value or impact on patient management [22]. Indeed, many of these technologies will never progress further as they are unable to overcome the challenges of becoming a 'product' [23,24]. These challenges include biological, technical, clinical and outcome validation [25]. As such, within this section, we

concentrate on techniques that utilise equipment commonly available in the hospital setting – in particular MRI and positron emission tomography (PET) modalities, which can today go beyond anatomical assessment and interrogate the microstructural, functional and/or metabolic properties of cancer.

3.1. Diffusion-weighted MRI

Diffusion-weighted MRI gives insight into tissue microstructure. In its most commonly implemented form, it interrogates tissue cellularity [26–28]: diffusion-weighted imaging (DWI) signal intensity is increased in most cancers due to the hindered translational motion of water molecules caused by high cellularity. The degree to which an image is sensitised to water diffusion is controlled by the operator by means of setting a 'b-value' (commonly set between 0 and 2000 s·mm^{-2}); a product of the amplitude, duration and timing of diffusion-sensitising magnetic field gradients is applied during signal generation.

Whilst DWI images are often visually assessed, the signal intensity of images acquired with increasing b-values is also exponentially fitted to allow quantitation of the apparent diffusion coefficient (ADC). ADC values are typically lower in malignant tissue when compared to surrounding normal tissue. In clinical practice, DWI has shown value in tumour detection, staging and treatment follow-up (including immune therapies) [29,30]. Furthermore, the ADC, and the ADC ratio of the lesion compared to the neighbouring tissue, is able to predict the Gleason grading of PCa lesions [31].

3.2. Dynamic contrast-enhanced MRI

Dynamic contrast enhancement-MRI (DCE-MRI) enables the assessment of microvasculature of the lesion; for cancer, it enables assessment of neovascularisation [32]. Tumour vasculature is characterised by a chaotic structure, a high number of dysfunctional vessels, complex branching patterns, abnormal permeability and nonuniform vascular densities, together resulting in blood flow that is spatially and temporally heterogeneous [33]. DCE-MRI evaluates this by using contrast agents that cause signal changes dependent on changes in blood flow, capillary density, permeability and extravascular-space volume induced by cancer. Fast T1-weighted MRI sequences are used to acquire repeated images depicting the signal changes that occur with the arrival and washout of contrast within a particular region, with a rapid enhancement and washout being typical of most cancers. DCE images

can be visually assessed and analysed through signal-intensity time curves or through models which quantify pharmacokinetic parameters (e.g. K^{trans}, K_{ep}, v_e; see below).

Qualitative assessment of DCE images relies upon localising regions of early enhancement and washout when compared to surrounding normal tissue. Signal-intensity time curves are generated through region of interest (ROI) placement and temporal extraction of mean ROI signal across sequential T1-weighted acquisitions. Time to start of enhancement, time to peak enhancement, maximum enhancement, slope of enhancement and area under the curve metrics can be derived and related to tissue vascular structure [34,35]. The most commonly used pharmacokinetic model (Tofts model) fits the signal-intensity time curves to a one-compartment model, allowing the calculation of extravascular extracellular space volume (v_e) and a transfer constant (K^{trans}, a measure of proportionality of distribution of contrast between the vascular and extravascular extracellular space). The vascular compartment volume is ignored as, for most cases, it is a relatively small fraction (1–10%) of the tissue [36–38]. Quantitative DCE-MRI is used within clinical trials as an endpoint for drug efficacy [21]; curve-shape assessment is routinely utilised clinically for breast imaging [39]; and visual assessment is recommended for the evaluation of PCa [40,41].

3.3. Magnetic resonance spectroscopy

Clinically applied magnetic resonance spectroscopy (MRS) techniques are not strictly an emerging entity and have been trialled since the availability of clinical-grade MRI scanners. They enable the generation and separation of MR signals from ^{1}H nuclei from different metabolites. Differences in the electron shielding of the ^{1}H nucleus between metabolites cause distinct frequencies of signal for individual metabolites [42]. However, the concentration of metabolites is many magnitudes smaller than the concentration of water within the body, and therefore, high-field magnets, long imaging times and a nonlocalised signal are commonly required to achieve metabolite signal-to-noise ratios sufficient for interpretation. These limitations, together with the limited availability of expertise to set up and process spectroscopy data, have meant that MRS is not widely employed in the clinical imaging of cancer. Nonetheless, metabolites in the millimolar range (including choline, creatine, lactate and citrate) are detectable and have been clinically evaluated within limited cancer applications. For instance, choline, a metabolic marker of cell membrane synthesis

and repair found in more rapidly proliferating cells, has been demonstrated to be a characteristic signature of more aggressive tumours [43]. Although no longer part of the standard PCa multiparametric imaging protocol, when used in combination with T2-MRI and DCE-MRI, sensitivities for tumour detection are higher [44].

3.4. Positron emission technology

Positron emission technology is a molecular imaging technique that can provide high sensitivity through use of positron emitters to label key molecules that are intravenously injected and their distribution and uptake imaged to provide insight into metabolic changes associated with cancer. Whilst PET scans can be viewed alone, because of their limited morphological detail hybrid instruments are commonly used to combine anatomical CT or MRI images with PET metabolic information [45,46].

4. Novel imaging methods

Despite the now almost routine use of the techniques discussed above [e.g. Mp-MRI for PCa using DWI and DCE imaging [47,48], staging of breast cancer using fludeoxyglucose (^{18}F) (FDG)]-PET [49] or evaluation of brain tumours using MRS) [50,51], the challenges of limited sensitivity, specificity, tumour characterisation and prognostication have not been fully addressed. Therefore, there is still considerable effort directed towards developing new and improved imaging methods. This section outlines a selection of novel approaches that have demonstrated promising initial results.

4.1. Machine learning applied to currently available cancer imaging techniques

The general supposition of machine learning (ML), when applied to radiology, is that images contain information on pathology which can be extracted by a computer algorithm with performance either as good as or better than a human. A set of images with a known ground truth (training set) are used to train an ML system so that, when new images (test set) are shown to the system, it can make a prediction based on its previous experience. This approach has been very successful for natural image analysis, even surpassing human ability in some tasks [52]. These same methods are being developed for medical imaging to improve the efficacy and efficiency of cancer detection and characterisation. ML can utilise quantitative

metrics, referred to as radiomic features, such as shape, uptake values and other features, including second-order features (texture) [53].

There are two commonly investigated ML methods for medical image analysis: classical ML and deep learning (DL). Classical ML usually requires manual segmentation of lesions and extraction of quantitative imaging features such as shape, volume, histogram and texture from a training set. Those features are used to train the ML algorithm, which then uses statistical analysis to identify the optimal relationship between the imaging features in order to predict the desired outcome. There are multiple types of algorithms, such as decision trees [54], support vector machines and naïve Bayes, each of which may be better suited to individual tasks.

Deep learning, however, uses networks that in some way resemble neurons of the human brain, comprising multiple layers of interconnected artificial neurons. Each neuron acts as a simple classifier that gives an output based on the inputs from preceding neurons; often, there are a number of layers and hundreds of thousands of individual neurons in a single network (Fig. 1). During the training phase, these DL systems will automatically learn discriminating features without the need for an expert to manually segment tumours; however, much larger training sets are generally required. The output from these methods could be ordinal, such as cancer verses noncancer, or on a continuous scale, predicting the probability of cancer between zero and one, for example. Furthermore, the result could be applied to the whole image, a specified ROI or on a per-voxel basis. When an ML system is used by a radiologist to aid in interpretation, this is often called computer-aided diagnosis (CAD).

As an exemplar, in the case of Mp-MRI of prostate, for which there has been considerable recent interest in ML, multiple CAD systems have been evaluated across various settings. Some systems, which produce probability heatmaps that can be overlaid onto the MRI images and highlight areas of suspicion, have produced stand-alone performances equivalent to experienced radiologists [55,56]. Others, however, have demonstrated that, when radiologists use such heatmaps during reporting, they improved their sensitivity for clinically significant cancer by up to 10%, whilst maintaining specificity [57,58]. Similar systems have also decreased the interobserver variability between radiologists of varying experience [57,59]. Alternative CAD systems have been designed to improve the classification of lesions in order to reduce false positives and unnecessary biopsies, which is common for indeterminate lesions. Multiple studies have shown that
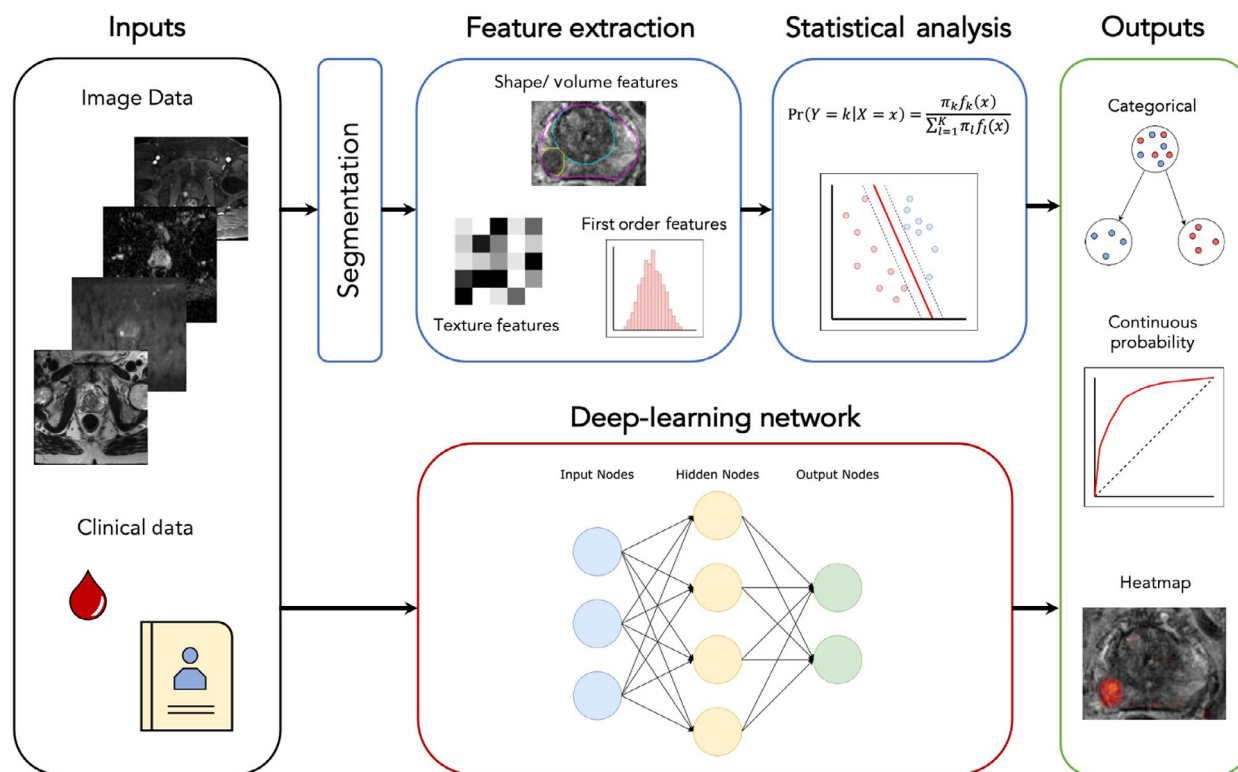
Fig. 1. Schematic diagram of common approaches to ML in medical imaging, from left to right. Inputs (black box) often include imaging DICOM (digital imaging and communications in medicine) data and clinical data. For classical ML (blue boxes), images are often segmented and radiomic features extracted for input into the chosen statistical analysis, whereas, for DL methods (red box), the neuronal network uses often unknown discriminating features found during training to classify patients into a specified output (green box), which could be a categorical group or a continuous probability where a receiver operating curve may be produced and, if analysis is done on a voxel-by-voxel basis, a heatmap can be constructed.

classical ML methods can better characterise suspicious lesions than radiologists [60–62], with Dinh *et al.* [62] significantly improving per-lesion specificity by 30% for detecting Gleason 3 + 4 cancer in 129 patients.

At this stage, these positive results are largely limited in generalisability due to similarities in their training and test data sets. For example, we know prostate Mp-MRI images from different institutions and scanner vendors can look markedly different; therefore, CAD systems need to be trained with large amounts of heterogeneous data in order to be robust enough for widespread clinical use. Gaur *et al.* [59] used a truly external and heterogeneous test set across five institutions and three MR vendors, demonstrating good performance, with the addition of their CAD system similar to with radiologists alone. This proves that CAD systems have the potential to be generalisable, but practical obstacles in obtaining large amounts of well-labelled heterogeneous data have limited progress in this area. Subsequently, these systems

will need to be prospectively assessed for important patient outcomes before CAD becomes part of the diagnostic pathway. Furthermore, DL and ML methods are still often viewed as 'black boxes' by clinicians, due to the difficultly in understanding how these techniques arrive at their conclusions [53]. The situation described for PCa imaging is replicated in the field of other cancers, for example breast and colon [63–65]. These imaging features can be further combined with genetic and clinical information and, together, can perform optimally [66].

4.2. Microstructural imaging with tissue model focused MRI

Clinically available microstructural MRI of cancer is reliant on a simple DWI [29], as described above. This conventional method is commonly applied to a range of cancer and noncancer applications (e.g. assessment of inflammatory changes in the bowel [67,68]) and, as such, is not tissue specific, with multiple pathological

mechanisms contributing to signal change. Consequently, whilst standard DWI is an improvement over anatomical imaging alone, it still lacks specificity [69]. One approach to address this is through development of 'intelligent MRI'; here, unlike the application of a general MRI technique to assess multiple pathologies, individual MRI techniques are crafted to gather specific signals from tissue that are then fed into mathematical models of cancer, in theory allowing a more nuanced assessment of the tissue microstructure [70]. Two such examples, both initially developed for PCa imaging, are highlighted here.

4.2.1. Vascular, extracellular and restricted diffusion for cytometry in tumours MRI

Vascular, extracellular and restricted diffusion for cytometry in tumours (VERDICT) is an imaging technique that builds upon conventional DWI. Initially developed for PCa assessment, VERDICT uses a mathematical model that has three main tissue compartments [71]. These compartments describe the diffusion signal in three separate populations: water molecules trapped inside cells, in the interstitium and inside blood vessels. Similar to conventional DWI, VERDICT MRI acquisition uses clinically available MRI scanners to acquire images with differing b-values (up to b3000 s·mm^2), the specific b-values having been selected from more detailed prior acquisitions to maximise sensitivity to histopathological changes induced by cancer balanced against maintaining a clinically feasible scan time [72]. The acquired data are then fitted to the mathematical model to generate microarchitectural parameters such as intracellular volume fraction (water inside cells), vascular fraction (water inside vessels) and extracellular extravascular fraction (water in the interstitium). Furthermore, estimates of cell radius can also be obtained from this technique.

Similar to many biomarkers, VERDICT MRI was first investigated in animal models. A murine xenograft model of colorectal cancer underwent VERDICT MRI before and after treatment with a chemotherapeutic agent. The study showed that VERDICT MRI could identify significant changes in cell size and vasculature after the administration of a chemotherapeutic agent, in contrast to standard ADC and other diffusion models [71].

Following on from animal work, the technique was tested in eight patients with biopsy-positive PCa. This feasibility study showed that VERDICT could distinguish between benign and cancerous regions found on biopsy [73]. To obtain further histopathological validation, VERDICT MRI was studied in five patients undergoing prostatectomy. This study showed a strong correlation between VERDICT microstructural parameters such as cellular fraction and collagen fibre patterns in the interstitium to histopathological parameters derived from *ex-vivo* prostatectomy specimens [74].

Based on the findings from these early studies, VERDICT MRI is being evaluated in a larger cohort of patients as part of the INNOVATE trial [75], a prospective single-centre study in 365 men suspected of having PCa who undergo VERDICT MRI before biopsy. The aim is to investigate whether VERDICT MRI can improve specificity of clinical Mp-MRI by reducing the number of indeterminate results. Repeatability and early efficacy of VERDICT MRI was studied in a subset of these patients. This study showed that the VERDICT parameter intracellular fraction (f_{IC}) was highly repeatable (ICC: 0.87–0.95) and showed potential in differentiating between benign and clinically significant cancer better than ADC [72]. The results of the full trial are awaited.

Outside of the prostate, VERDICT MRI has also shown promise in the characterisation of brain gliomas and bone metastases compared with existing DWI [76,77]. As an imaging biomarker, it is in the early clinical validation phase, and further work is needed to establish multicentre reproducibility and clinical impact (Fig. 2).

4.2.2. Luminal water fraction imaging

Luminal water fraction imaging (LWF) imaging is an MRI technique that has also been developed within the setting of PCa. Here, the mathematical tissue model distinguishes the luminal space of prostate tissue from the stroma and epithelia. In contrast to VERDICT MRI, which is based on DWI, LWF MRI requires multiple T2-weighted images at differing echo times to populate signals into the model [78]. In pure water, T2 relaxation (the predominant process through which MRI signal decays on T2-weighted images) is mono-exponential. However, in the case of prostate tissue, T2 relaxation from fluid contained within microstructural ducts and acini decays significantly more slowly that from the water contained within the surrounding stroma [79], forming two distinct Gaussian distributions of T2 relaxation times. Signal from multiple increasingly T2-weighted images is input into a mathematical model that separates these two distributions [80] into T-long, corresponding to the glandular/intraluminal region, and T-short, which corresponds to the cellular/extraluminal region. An LWF map can then be derived as a fraction volume of luminal space within the tissue (T-long/(T-
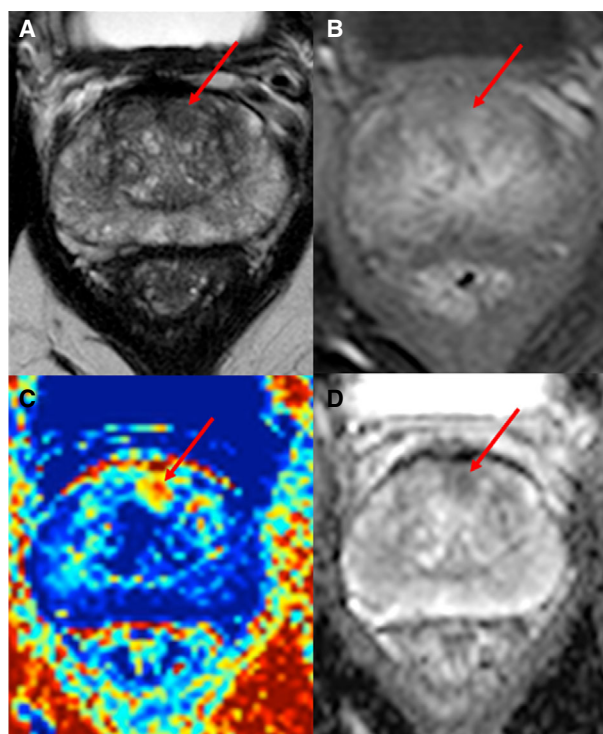
Fig. 2. MRI images of a 58 years old with biopsy-proven PCa. (A) An axial T2-weighted MRI image showing a focus of homogeneous low signal (red arrow) in the left anterior para-midline transition zone. (B) T1-weighted, fat-suppressed, postcontrast image showing focal enhancement (red arrow) in the left anterior transition zone. (C) VERDICT intracellular volume fraction (FIC) map showing a focal area with increased FIC (red arrow), which enables clearer definition of the biopsy-positive tumour. (D) ADC map showing reduced signal intensity in the tumour (red arrow).

long + T-short) component [78]). As luminal space is reduced in PCa, with loss of luminal space correlated with increased Gleason tumour grade, LWF MRI has merit for both cancer detection and characterisation (Fig. 3). Initially requiring the acquisition of 64 different signals to calculate, a simplified version utilising a reduced number of T2-weighted signals has been shown to perform well for cancer detection and characterisation [81].

Luminal water fraction imaging is relatively early in its developmental phase as compared to VERDICT MRI, but its reliance on T2-weighted imaging has the potential advantage of avoiding common artefacts that degrade image quality of DWI-based techniques. Currently, however, LWF studies are all single-centre studies within PCa, with a limited number of subjects; however, the initial clinical validation in these studies shows promise [81]. With ongoing development, LWF could also be applied to the assessment of other glandular organs (e.g. breast and pancreas) for cancer evaluation.

4.3. Emerging techniques for metabolic assessment of cancer

There are a number of opportunities to assess cancer metabolism. Novel PET tracers have the potential to provide specificity and exquisite sensitivity to disease [82], whilst new spectroscopic MRI methods utilising hyperpolarised ^{13}C-labelled substrates pave the way to dynamic assessment of tumour metabolism [83].

4.3.1. PET imaging tracers

Fludeoxyglucose (^{18}F) is the most widely used tracer in PET-based imaging and has shown utility in multiple cancer types at different stages of management. In the case of non-small-cell lung cancer, FDG-PET/CT has shown an improvement in staging when compared to CT alone, and utility as a significant prognostication marker, which ultimately leads to changes in clinical management [84–86]. However, for some cancers, the utility of FDG as an indicator of increased cellular metabolism has limited indications because of inherent biological features of the cancer or because of technical limitations, such as in the case of PCa and renal cell carcinomas, among others [87–90]. Therefore, multiple tracers have been developed in order to assess other metabolic pathways in cancer and other pathologies.

Choline is one such tracer that exploits the increased cell membrane turnover of malignant cells, resulting in increased choline uptake to be used as a precursor for the biosynthesis of phospholipids [91–93]. Choline tracing has been largely used in PCa and is found to have a sensitivity and specificity of 85.6% and 92.6%, respectively, for all metastatic sites, and is thus advocated for use in the biochemical recurrence setting [94]. Furthermore, potential utility of choline PET has been investigated in multiple myeloma and hepatocellular carcinoma and has shown promise [95,96].

Tracers that currently show great promise largely in the setting of biochemical recurrence of PCa but also potentially in the initial staging of higher risk cancers are prostate-specific membrane antigen (PSMA) and fluorine-18(^{18}F)-fluciclovine. Fluciclovine is an amino acid analogue that is taken up in greater quantities by PCa cells when compared to surrounding normal tissue, and has been shown to be effective in the early detection of nodal and distant metastasis in recurrent prostate disease, detecting lesions in 57% of patients (122/213) with biochemical recurrence that had equivocal or negative standard of care imaging (abdominopelvic CT or MRI and bone scintigraphy) [97].

Instead, PSMA is a receptor on the cell surface of the prostate cells and increases in density with higher-
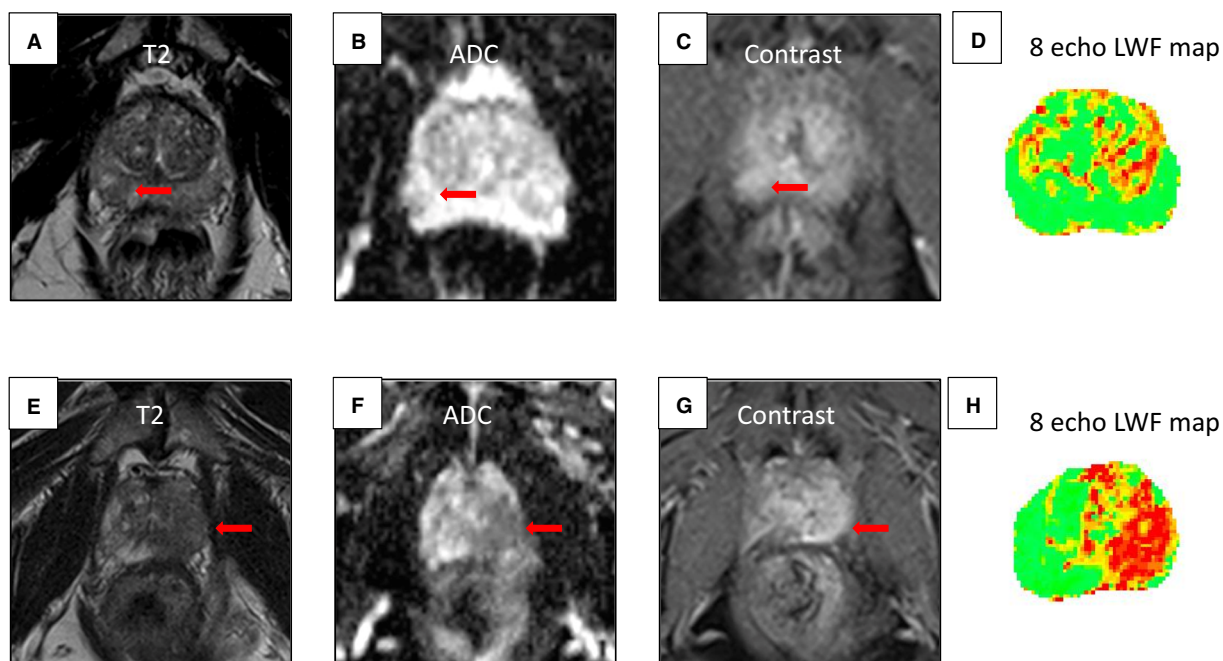
Fig. 3. Comparison of conspicuous standard MRI lesions with luminal water fraction (LWF) imaging mapping and targeted biopsy. Lesion indicated by red arrow. Top row from left to right: 65-year-old man with PSA 9.9: (A) T2-weighted MRI showing a region of lesion with reduced signal intensity right periphery. (B) ADC map showing reduced signal intensity in the lesion. (C) Dynamic contrast-enhanced (DCE) image showing increased signal intensity at the lesion. A Likert score of 4 was given. (D) LWF imaging mapping, which does not indicate the presence of a lesion. Biopsy result: benign. Bottom row from left to right: 68-year-old man with PSA 14: (E) T2-weighted MRI showing a region of reduced signal in the left peripheral zone extending to the transitional zone. (F) ADC mapping, showing reduced signal intensity at the peripheral lesion. (G) DCE imaging, showing lesion enhancement. A Likert score of 5 was given. (H) LWF mapping was positive at the lesion. Biopsy result: positive for cancer Gleason 4 + 3.

grade tumours, metastasis and hormone-refractory PCa. The precise function is not known, and it is also detected in smaller levels in the small intestine and brain [98,99]. PSMA PET is characterised by having exceptional node metastasis detection specificities, reaching 99%, significantly outperforming other PET-CT techniques, and is furthermore not limited to size criteria [100]. Additionally, PSMA PET/CT has greater sensitivities in the detection of bone metastasis when compared to whole-body bone scans, in one study doubling the number of bone metastases detected [101]. Most significantly, in the setting of biochemical recurrence following radical prostatectomy, PSMA PET/CT showed a detection efficacy of 96.8% for PSA values > 2 and, notably, detection rates of 67% for PSA values < 1, which is markedly better than choline-based PET/CT, with rates ranging from 19% to 36% [102]. Therefore, PSMA PET/CT has shown utility most significantly in biochemical recurrence. However, there are some limitations, as it is not funded by many healthcare providers and it has been

shown that, in very advanced disease, PSMA expression may be lost [103].

4.3.2. Hyperpolarised MRI

Carbon serves as the backbone of nearly all organic molecules, and MRI signal can be generated from ^{13}C nuclei, making carbon an attractive target for imaging. However, ^{13}C imaging remains technically challenging. First, the natural abundance of ^{13}C is only 1.1% when compared to 99% for ^{1}H, which is used to generate signal for conventional MRI (Fig. 4). Therefore, ^{13}C probes are synthetically enriched to increase the concentration of ^{13}C, typically to 99%, and, through the process of hyperpolarisation, the MR signal of ^{13}C-labelled substrates is boosted by a factor >10 000 [104]. This typically allows 35–40 mL of hyperpolarised substrate in solution to provide sufficient signal following intravenous injection [105]. Once the dissolute is ready for injection, the hyperpolarised state (and hence signal) for 1-^{13}C-pyruvate decays rapidly,
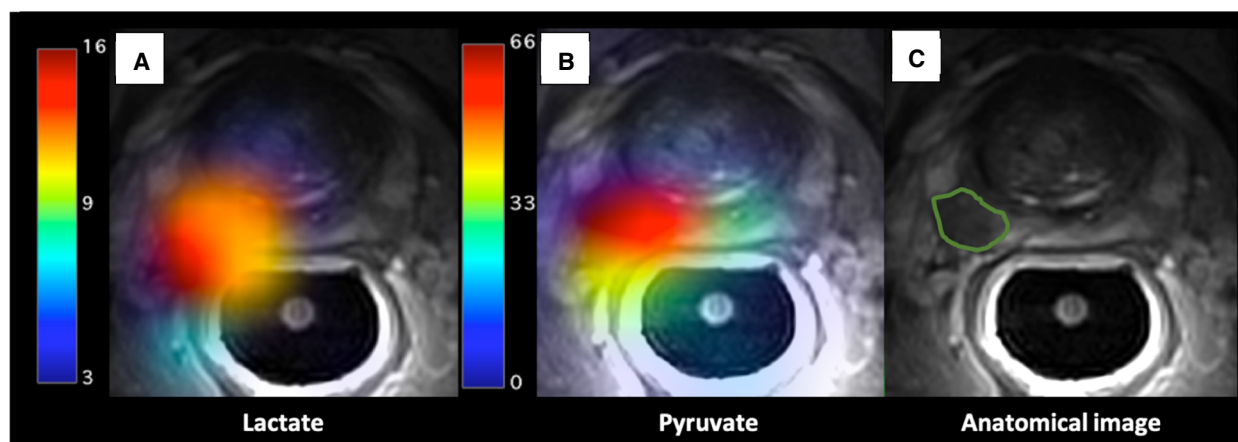
Fig. 4. Hyperpolarised 1-^{13}C-pyruvate-MRI metabolite maps in MRI- and biopsy-positive PCa. Axial T2-weighted ^{1}H-MRI scan of a subject with right-sided, posterior, biopsy-confirmed Gleason 4 + 3 PCa, segmented in a green line in panel C. Images were acquired with a receive-only endorectal coil (RAPID Biomedical). Maps of 1-^{13}C-pyruvate (centre, panel B) and 1-^{13}C-lactate (left, panel A) were produced, via an IDEAL model, from multiecho-bSSFP data (13C-MRI) and overlaid on the original T2W acquisition; demonstrating the distribution of hyperpolarised 1-^{13}C-pyruvate (panel B) and its downstream metabolites, (lactate in panel A) 25 s after contrast injection.

with a half-life of 45–60 s [104,106,107]. Injection and imaging must therefore be rapidly completed, ideally within 2–3 min. This poses a number of technical and logistical challenges [83], limiting the current use of hyperpolarised methods to research within specialised centres.

Whilst a number of hyperpolarised substrates are available in the preclinical setting [108], to date only hyperpolarised ^{13}C-labelled pyruvate has been trialled in humans [109–113]. Pyruvate is the end product of glycolysis and can be converted to lactate via the enzyme lactate dehydrogenase or to alanine by alanine transaminase. Pyruvate can also be transported into the mitochondria, where it is converted to acetyl-CoA CO_2 by pyruvate dehydrogenase. As such, following injection of hyperpolarised 1-^{13}C-pyruvate, an MRI signal is typically observed from lactate, alanine and/or bicarbonate dependent on tissue and pathology [114]. Typically, imaging is performed with a temporal resolution of 3–6 s, allowing for dynamic changes in the strengths of signals from pyruvate and its downstream products to be documented, and thereby for enzymatic fluxes to be interrogated [107,113].

Human dose escalation and safety study of hyperpolarised 1-^{13}C-pyruvate were reported in 2013 [105]. Since then, there have been a number of reported first-in-human clinical applications, including prostate, renal and breast cancer [105,115,116]. Immunohistochemical analysis of tumour regions detected with 1-^{13}C-pyruvate hyperpolarised MRI (HP-MRI) confirms an overexpression of monocarboxylate transport 1, which imports pyruvate and lactate into cells [112].

As well as detection and potential evaluation of disease aggressiveness of PCa [112,117], 1-^{13}C-pyruvate HP-MRI has also demonstrated proof of concept as a metabolic response biomarker to androgen-deprivation therapy [113].

HP-MRI has the potential to provide nonradioactive and unique-in-human dynamic assessment of tumour metabolism, providing opportunities for tumour detection, characterisation and treatment response assessment. Currently, it is in the very early stages of development and will likely need: (a) advances in hyperpolariser hardware to reduce cost and complexity [118] and (b) implementation of methods to prolong the hyperpolarised state [119] if it is to enter widespread clinical use.

5. Conclusion

Major technological advances have been made in the last 2 decades that have provided new radiological tools with which to interrogate cancer. Anatomical imaging remains the mainstay for the assessment of disease and treatment response [120,121], but new clinically available MRI techniques that can evaluate tumour cellularity and vascularity are now commonly utilised for selected tumours, with PCa being used in this exemplar [14,122,123]. Imaging can yet do more, and new research is emerging on methods that improve the microstructural detail that imaging can depict [70] together with moving into the assessment of metabolic processes, in some cases in real time [124]. Through careful and methodological development,

these techniques may provide clinicians more sensitive and specific markers for cancer assessment.

Conflict of interest

The authors declare no conflict of interest.

Author contributions

AR first author of manuscript. FG, TS, SS and SA contributed to manuscript including image and diagram development. SP conceived, supervised, edited and contributed to manuscript.

References

1 Cavanagh P & Royal College of Radiologists (2014) Recommendations for Cross-sectional Imaging in Cancer Management. 2nd edn, Ref No. BFCR(14)2. The Royal College of Radiologists, London, UK.

2 Dwamena BA, Sonnad SS, Angobaldo JO & Wahl RL (1999) Metastases from non-small cell lung cancer: mediastinal staging in the 1990s - Meta-analytic comparison of PET and CT. *Radiology* **213**, 530–536.

3 Curtin HD, Ishwaran H, Mancuso AA, Dalley RW, Caudry DJ & McNeil BJ (1998) Comparison of CT and MR imaging in staging of neck metastases. *Radiology* **207**, 123–130.

4 Wang H, Li QK, Auster M & Gong G (2018) PET and CT features differentiating infectious/inflammatory from malignant mediastinal lymphadenopathy: a correlated study with endobronchial ultrasound-guided transbronchial needle aspiration. *Radiol Infect Dis* **5**, 7–13.

5 Eisenhauer EA, Therasse P, Bogaerts J, Schwartz LH, Sargent D, Ford R, Dancey J, Arbuck S, Gwyther S, Mooney M *et al.* (2009) New response evaluation criteria in solid tumours: revised RECIST guideline (version 1.1). *Eur J Cancer* **45**, 228–247.

6 Tirkes T, Hollar MA, Tann M, Kohli MD, Akisik F & Sandrasegaran K (2013) Response criteria in oncologic imaging: review of traditional and new criteria. *Radiographics* **33**, 1323–1341.

7 Schliep S, Agaimy A, Cavallaro A, Kiesewetter F, Schuler G & Heinzerling L (2018) Concealed complete response in melanoma patients under therapy with immune checkpoint inhibitors: two case reports. *J Immunother Cancer* **6**, 4–7.

8 Giganti F, Rosenkrantz AB, Villeirs G, Panebianco V, Stabile A, Emberton M & Moore CM (2019) The evolution of MRI of the prostate: the past, the present, and the future. *Am J Roentgenol* **213**, 384–396.

9 Bangma CH, Roemeling S & Schröder FH (2007) Overdiagnosis and overtreatment of early detected prostate cancer. *World J Urol* **25**, 3–9.

10 El-Shater Bosaily A, Parker C, Brown LC, Gabe R, Hindley RG, Kaplan R, Emberton M & Ahmed HU (2015) PROMIS - prostate MR imaging study: a paired validating cohort study evaluating the role of multi-parametric MRI in men with clinical suspicion of prostate cancer. *Contemp Clin Trials* **42**, 26–40.

11 Barzell WE & Melamed MR (2007) Appropriate patient selection in the focal treatment of prostate cancer: the role of transperineal 3-dimensional pathologic mapping of the prostate-a 4-year experience. *Urology* **70**, 27–35.

12 Onik G, Miessau M & Bostwick DG (2009) Three-dimensional prostate mapping biopsy has a potentially significant impact on prostate cancer management. *J Clin Oncol* **27**, 4321–4326.

13 Loeb S, Vellekoop A, Ahmed HU, Catto J, Emberton M, Nam R, Rosario DJ, Scattoni V & Lotan Y (2013) Systematic review of complications of prostate biopsy. *Eur Urol* **64**, 876–892.

14 National Institute for Health and Care Excellence (NICE). Clinical guideline (NG131). NICE website, 2019. www.nice.org.uk/guidance/ng131. Accessed May 17 2020. https://doi.org/10.1016/S0140-6736(96)07393-X

15 Ahmed HU, El-Shater Bosaily A, Brown LC, Gabe R, Kaplan R, Parmar MK, Collaco-Moraes Y, Ward K, Hindley RG, Freeman A *et al.* (2017) Diagnostic accuracy of multi-parametric MRI and TRUS biopsy in prostate cancer (PROMIS): a paired validating confirmatory study. *Lancet* **389**, 815–822.

16 Kasivisvanathan V, Rannikko AS, Borghi M, Panebianco V, Mynderse LA, Vaarala MH, Briganti A, Budäus L, Hellawell G, Hindley RG *et al.* (2018) MRI-targeted or standard biopsy for prostate-cancer diagnosis. *N Engl J Med* **378**, 1767–1777.

17 van der Leest M, Cornel E, Israël B, Hendriks R, Padhani AR, Hoogenboom M, Zamecnik P, Bakker D, Setiasti AY, Veltman J *et al.* (2019) Head-to-head comparison of transrectal ultrasound-guided prostate biopsy versus multiparametric prostate resonance imaging with subsequent magnetic resonance-guided biopsy in biopsy-naïve men with elevated prostate-specific antigen: a large prospective Mu. *Eur Urol* **75**, 570–578.

18 Rouvière O, Puech P, Renard-Penna R, Claudon M, Roy C, Mège-Lechevallier F, Decaussin-Petrucci M, Dubreuil-Chambardel M, Magaud L, Remontet L *et al.* (2019) Use of prostate systematic and targeted biopsy on the basis of multiparametric MRI in biopsy-naive patients (MRI-FIRST): a prospective, multicentre, paired diagnostic study. *Lancet Oncol* **20**, 100–109.

19 O'Connor JPB, Boult JKR, Jamin Y, Babur M, Finegan KG, Williams KJ, Little RA, Jackson A, Parker GJM, Reynolds AR *et al.* (2016) Oxygen-enhanced MRI accurately identifies, quantifies, and maps tumor hypoxia in preclinical cancer models. *Cancer Res* **76**, 787–795.

20 Bernsen MR, Kooiman K, Segbers M, van Leeuwen FWB & de Jong M (2015) Biomarkers in preclinical cancer imaging. *Eur J Nucl Med Mol Imaging* **42**, 579–596.

21 O'Connor JPB, Jackson A, Parker GJM, Roberts C & Jayson GC (2012) Dynamic contrast-enhanced MRI in clinical trials of antivascular therapies. *Nat Rev Clin Oncol* **9**, 167–177.

22 Hayes DF, Allen J, Compton C, Gustavsen G, Leonard DGB, McCormack R, Newcomer L, Pothier K, Ransohoff D, Schilsky RL *et al.* (2013) Breaking a vicious cycle. *Sci Transl Med* **5**, 1–8.

23 Macleod MR, Michie S, Roberts I, Dirnagl U, Chalmers I, Ioannidis JPA, Al-Shahi Salman R, Chan AW & Glasziou P (2014) Biomedical research: increasing value, reducing waste. *Lancet* **383**, 101–104.

24 O'Connor JPB, Aboagye EO, Adams JE, Aerts HJWL, Barrington SF, Beer AJ, Boellaard R, Bohndiek SE, Brady M, Brown G *et al.* (2017) Imaging biomarker roadmap for cancer studies. *Nat Rev Clin Oncol* **14**, 169–186.

25 Waterton JC & Pylkkanen L (2012) Qualification of imaging biomarkers for oncology drug development. *Eur J Cancer* **48**, 409–415.

26 Fliedner FP, Engel TB, El-Ali HH, Hansen AE & Kjaer A (2020) Diffusion weighted magnetic resonance imaging (DW-MRI) as a non-invasive, tissue cellularity marker to monitor cancer treatment response. *BMC Cancer* **20**, 1–9.

27 Hagmann P, Jonasson L, Maeder P, Thiran JP, Wedeen VJ & Meuli R (2006) Understanding diffusion MR imaging techniques: from scalar diffusion-weighted imaging to diffusion tensor imaging and beyond. *Radiographics* **26**, 205–224.

28 Surov A, Meyer HJ & Wienke A (2017) Correlation between apparent diffusion coefficient (ADC) and cellularity is different in several tumors: a meta-analysis. *Oncotarget* **8**, 59492–59499.

29 Koh DM & Collins DJ (2007) Diffusion-weighted MRI in the body: applications and challenges in oncology. *Am J Roentgenol* **188**, 1622–1635.

30 Koh DM, Blackledge M, Collins DJ, Padhani AR, Wallace T, Wilton B, Taylor NJ, Stirling JJ, Sinha R, Walicke P *et al.* (2009) Reproducibility and changes in the apparent diffusion coefficients of solid tumours treated with combretastatin A4 phosphate and bevacizumab in a two-centre phase I clinical trial. *Eur Radiol* **19**, 2728–2738.

31 De Cobelli F, Ravelli S, Esposito A, Giganti F, Gallina A, Montorsi F & Del Maschio A (2015) Apparent diffusion coefficient value and ratio as noninvasive potential biomarkers to predict prostate cancer grading: comparison with prostate biopsy and radical prostatectomy specimen. *Am J Roentgenol* **204**, 550–557.

32 O'Neill AC, Alessandrino F, Tirumani SH & Ramaiya NH (2018) Hallmarks of cancer in the reading room: a guide for radiologists. *Am J Roentgenol* **211**, 470–484.

33 García-Figueiras R, Padhani AR, Beer AJ, Baleato-González S, Vilanova JC, Luna A, Oleaga L, Gómez-Caamaño A & Koh DM (2015) Imaging of tumor angiogenesis for radiologists-part 1: biological and technical basis. *Curr Probl Diagn Radiol* **44**, 407–424.

34 Paldino MJ & Barboriak DP (2009) Fundamentals of quantitative dynamic contrast-enhanced MR imaging. *Magn Reson Imaging Clin N Am* **17**, 277–289.

35 Jackson A, O'Connor JPB, Parker GJM & Jayson GC (2007) Imaging tumor vascular heterogeneity and angiogenesis using dynamic contrast-enhanced magnetic resonance imaging. *Clin Cancer Res* **13**, 3449–3459.

36 Tofts PS, Brix G, Buckley DL, Evelhoch JL, Henderson E, Knopp MV, Larsson HBW, Lee T-Y, Mayr NA, Parker GJM *et al.* (1999) Estimating kinetic parameters from dynamic contrast-enhanced T1-weighted MRI of a diffusable tracer: standardized quantities and symbols. *J Magn Reson Imaging* **10**, 223–232.

37 Tofts PS & Kermode AG (1991) Measurement of the blood-brain barrier permeability and leakage space using dynamic MR imaging. 1. Fundamental concepts. *Magn Reson Med* **17**, 357–367.

38 Tofts P (2010) T1-weighted DCE imaging concepts: modelling, acquisition and analysis. *Signal* **500**, 400.

39 El Khouli RH, Macura KJ, Jacobs MA, Khalil TH, Kamel IR, Dwyer A & Bluemke DA (2009) Dynamic contrast-enhanced MRI of the breast: quantitative method for kinetic curve type assessment. *Am J Roentgenol* **193**, 1–15.

40 Sabouri S, Chang SD, Goldenberg SL, Savdie R, Jones EC, Black PC, Fazli L & Kozlowski P (2019) Comparing diagnostic accuracy of luminal water imaging with diffusion-weighted and dynamic contrast-enhanced MRI in prostate cancer: a quantitative MRI study. *NMR Biomed* **32**, 1–10.

41 Jackson ASN, Reinsberg SA, Sohaib SA, Charles-edwards EM, Jhavar S, Christmas TJ, Thompson AC, Bailey MJ, Corbishley CM, Fisher C *et al.* (2009) Dynamic contrast-enhanced MRI for prostate cancer localization. *Br J Radiol* **82**, 148–156.

42 Qayyum A (2009) MR spectroscopy of the liver: principles and clinical applications. *Radiographics* **29**, 1653–1664.

43 García-Figueiras R, Baleato-González S, Padhani AR, Luna-Alcalá A, Vallejo-Casas JA, Sala E, Vilanova JC, Koh DM, Herranz-Carnero M & Vargas HA (2019) How clinical imaging can assess cancer biology. *Insights Imaging* **10**, 28. https://doi.org/10.1186/s13244-019-0703-0

44 Turkbey B, Pinto PA, Mani H, Bernardo M, Pang Y, McKinney YL, Khurana K, Ravizzini GC, Albert PS, Merino MJ *et al.* (2010) Prostate cancer: value of multiparametric MR imaging at 3 T for detection - histopathologic correlation. *Radiology* **255**, 89–99.

45 Berlin L (1994) Fundamentals of diagnostic radiology. *Radiology* **192**, 66.

46 Zhu A & Shim H (2011) Current molecular imaging positron emitting radiotracers in oncology. *Nucl Med Mol Imaging* **45**, 1–14.

47 Stabile A, Giganti F, Rosenkrantz AB, Taneja SS, Villeirs G, Gill IS, Allen C, Emberton M, Moore CM & Kasivisvanathan V (2020) Multiparametric MRI for prostate cancer diagnosis: current status and future directions. *Nat Rev Urol* **17**, 41–61.

48 Hoeks CMA, Barentsz JO, Hambrock T, Yakar D, Somford DM, Heijmink SWTPJ, Scheenen TWJ, Vos PC, Huisman H, van Oort IM *et al.* (2011) Prostate cancer: multiparametric MR imaging for detection, localization, and staging. *Radiology* **261**, 46–66.

49 Groheux D, Cochet A, Humbert O, Alberini JL, Hindié E & Mankoff D (2016) 18F-FDG PET/CT for staging and restaging of breast cancer. *J Nucl Med* **57**, 17S–26S.

50 Majós C, Aguilera C, Alonso J, Julià-Sapé M, Castañer S, Sánchez JJ, Samitier Á, León A, Rovira Á & Arús C (2009) Proton MR spectroscopy improves discrimination between tumor and pseudotumoral lesion in solid brain masses. *Am J Neuroradiol* **30**, 544–551.

51 Horská A & Barker PB (2010) Imaging of brain tumors: MR spectroscopy and metabolic imaging. *Neuroimaging Clin N Am* **20**, 293–310.

52 He K, Zhang X, Ren S & Sun J (2015) Deep residual learning for image recognition. *Proc IEEE Comput Soc Conf Comput Vis Pattern Recognit* **2016-Decem**, 770–778.

53 Avanzo M, Wei L, Stancanello J, Vallières M, Rao A, Morin O, Mattonen SA & El Naqa I (2020) Machine and deep learning methods for radiomics. *Med Phys* **47**, e185–e202.

54 El Naqa I, Ruan D, Valdes G, Dekker A, McNutt T, Ge Y, Wu QJ, Oh JH, Thor M, Smith W *et al.* (2018) Machine learning and modeling: data, validation, communication challenges. *Med Phys* **45**, e834–e840.

55 Schelb P, Kohl S, Radtke JP, Wiesenfarth M, Kickingereder P, Bickelhaupt S, Kuder TA, Stenzinger A, Hohenfellner M, Schlemmer H-P *et al.* (2019) Classification of cancer at prostate MRI: deep learning versus clinical PI-RADS assessment. *Radiology* **293**, 607–617.

56 Cao R, Mohammadian Bajgiran A, Afshari Mirak S, Shakeri S, Zhong X, Enzmann D, Raman S & Sung K (2019) Joint prostate cancer detection and Gleason score prediction in mp-MRI via FocalNet. *IEEE Trans Med Imaging* **38**, 2496–2506.

57 Giannini V, Mazzetti S, Armando E, Carabalona S, Russo F, Giacobbe A, Muto G & Regge D (2017) Multiparametric magnetic resonance imaging of the prostate with computer-aided detection: experienced observer performance study. *Eur Radiol* **27**, 4200–4208.

58 Zhu L, Gao G, Liu Y, Han C, Liu J, Zhang X & Wang X (2020) Feasibility of integrating computer-aided diagnosis with structured reports of prostate multiparametric MRI. *Clin Imaging* **60**, 123–130.

59 Gaur S, Lay N, Harmon SA, Doddakashi S, Mehralivand S, Argun B, Barrett T, Bednarova S, Girometti R, Karaarslan E *et al.* (2018) Can computer-aided diagnosis assist in the identification of prostate cancer on prostate MRI? A multi-center, multi-reader investigation. *Oncotarget* **9**, 33804–33817.

60 Niu XK, Chen ZF, Chen L, Li J, Peng T & Li X (2018) Clinical application of biparametric MRI texture analysis for detection and evaluation of high-grade prostate cancer in zone-specific regions. *Am J Roentgenol* **210**, 549–556.

61 Wang J, Wu CJ, Bao ML, Zhang J, Wang XN & Zhang YD (2017) Machine learning-based analysis of MR radiomics can help to improve the diagnostic performance of PI-RADS v2 in clinically relevant prostate cancer. *Eur Radiol* **27**, 4082–4090.

62 Dinh AH, Melodelima C, Souchon R, Moldovan PC, Bratan F, Pagnoux G, Mège-Lechevallier F, Ruffion A, Crouzet S, Colombel M *et al.* (2018) Characterization of prostate cancer with Gleason score of at least 7 by using quantitative multiparametric MR imaging: validation of a computer-aided diagnosis system in patients referred for prostate biopsy. *Radiology* **287**, 525–533.

63 Robinson C, Halligan S, Iinuma G, Topping W, Punwani S, Honeyfield L & Taylor SA (2011) CT colonography: computer-assisted detection of colorectal cancer. *Br J Radiol* **84**, 435–440.

64 Liu H, Wang J, Gao J, Liu S, Liu X, Zhao Z, Guo D & Dan G (2020) A comprehensive hierarchical classification based on multi-features of breast DCE-MRI for cancer diagnosis. *Med Biol Eng Comput* **58**, 2413–2425.

65 Antropova N, Huynh B & Giger M (2017) Performance comparison of deep learning and segmentation-based radiomic methods in the task of distinguishing benign and malignant breast lesions on DCE-MRI. *Med Imaging 2017 Comput Diagnosis* **10134**, 101341G.

66 Grossmann P, Stringfield O, El-Hachem N, Bui MM, Rios Velazquez E, Parmar C, Leijenaar RTH, Haibe-Kains B, Lambin P, Gillies RJ *et al.* (2017) Defining the biological basis of radiomic phenotypes in lung cancer. *Elife* **6**, 1–22.

67 Kilickesmez O, Atilla S, Soylu A, Tasdelen N, Bayramoglu S, Cimilli T & Gurmen N (2009) Diffusion-weighted imaging of the rectosigmoid colon: preliminary findings. *J Comput Assist Tomogr* **33**, 863–866.

68 Pouillon L, Laurent V, Pouillon M, Bossuyt P, Bonifacio C, Danese S, Deepak P, Loftus EV, Bruining DH & Peyrin-Biroulet L (2018) Diffusion-weighted MRI in inflammatory bowel disease. *Lancet Gastroenterol Hepatol* **3**, 433–443.

69 Yoshimitsu K, Kiyoshima K, Irie H, Tajima T, Asayama Y, Hirakawa M, Ishigami K, Naito S & Honda H (2008) Usefulness of apparent diffusion coefficient map in diagnosing prostate carcinoma: correlation with stepwise histopathology. *J Magn Reson Imaging* **27**, 132–139.

70 Le Bihan D, Breton E, Lallemand D, Aubin ML, Vignaud J & Laval-Jeantet M (1988) Separation of diffusion and perfusion in intravoxel incoherent motion MR imaging. *Radiology* **168**, 497–505.

71 Panagiotaki E, Walker-Samuel S, Siow B, Johnson SP, Rajkumar V, Pedley RB, Lythgoe MF & Alexander DC (2014) Noninvasive quantification of solid tumor microstructure using VERDICT MRI. *Cancer Res* **74**, 1902–1912.

72 Johnston EW, Bonet-Carne E, Ferizi U, Yvernault B, Pye H, Patel D, Clemente J, Piga W, Heavey S, Sidhu HS *et al.* (2019) VERDICT MRI for prostate cancer: intracellular volume fraction versus apparent diffusion coefficient. *Radiology* **291**, 391–397.

73 Panagiotaki E, Chan RW, Dikaios N, Ahmed HU, O'Callaghan J, Freeman A, Atkinson D, Punwani S, Hawkes DJ & Alexander DC (2015) Microstructural characterization of normal and malignant human prostate tissue with vascular, extracellular, and restricted diffusion for cytometry in tumours magnetic resonance imaging. *Invest Radiol* **50**, 218–227.

74 Bailey C, Bourne RM, Siow B, Johnston EW, Brizmohun Appayya M, Pye H, Heavey S, Mertzanidou T, Whitaker H, Freeman A *et al.* (2019) VERDICT MRI validation in fresh and fixed prostate specimens using patient-specific moulds for histological and MR alignment. *NMR Biomed* **32**, e4073.

75 Johnston E, Pye H, Bonet-Carne E, Panagiotaki E, Patel D, Galazi M, Heavey S, Carmona L, Freeman A, Trevisan G *et al.* (2016) INNOVATE: a prospective cohort study combining serum and urinary biomarkers with novel diffusion-weighted magnetic resonance imaging for the prediction and characterization of prostate cancer. *BMC Cancer* **16**, 816. https://doi.org/10.1186/s12885-016-2856-2

76 Zaccagna F, Riemer F, Priest AN, McLean MA, Allinson K, Grist JT, Dragos C, Matys T, Gillard JH, Watts C *et al.* (2019) Non-invasive assessment of glioma microstructure using VERDICT MRI: correlation with histology. *Eur Radiol* **29**, 5559–5566.

77 Bailey C, Collins DJ, Tunariu N, Orton MR, Morgan VA, Feiweier T, Hawkes DJ, Leach MO, Alexander DC & Panagiotaki E (2018) Microstructure characterization of bone metastases from prostate cancer with diffusion MRI: preliminary findings. *Front Oncol* **8**, 26. https://doi.org/10.3389/fonc.2018.00026

78 Sabouri S, Chang SD, Savdie R, Zhang J, Jones EC, Goldenberg SL, Black PC & Kozlowski P (2017) Luminal water imaging: a new MR imaging T2 mapping technique for prostate cancer diagnosis. *Radiology* **284**, 451–459.

79 Bourne RM, Kurniawan N, Cowin G, Stait-Gardner T, Sved P, Watson G, Chowdhury S & Price WS (2012) Biexponential diffusion decay in formalin-fixed prostate tissue: preliminary findings. *Magn Reson Med* **68**, 954–959.

80 Gilani N, Rosenkrantz AB, Malcolm P & Johnson G (2015) Minimization of errors in biexponential T2 measurements of the prostate. *J Magn Reson Imaging* **42**, 1072–1077.

81 Devine W, Giganti F, Johnston EW, Sidhu HS, Panagiotaki E, Punwani S, Alexander DC & Atkinson D (2019) Simplified luminal water imaging for the detection of prostate cancer from multiecho T2 MR images. *J Magn Reson Imaging* **50**, 910–917.

82 Pantaleo MA, Nannini M, Maleddu A, Fanti S, Ambrosini V, Nanni C, Boschi S & Biasco G (2008) Conventional and novel PET tracers for imaging in oncology in the era of molecular therapy. *Cancer Treat Rev* **34**, 103–121.

83 Wang ZJ, Ohliger MA, Larson PEZ, Gordon JW, Bok RA, Slater J, Villanueva-Meyer JE, Hess CP, Kurhanewicz J & Vigneron DB (2019) Hyperpolarized 13C MRI: state of the art and future directions. *Radiology* **291**, 273–284.

84 Im HJ, Pak K, Cheon GJ, Kang KW, Kim SJ, Kim IJ, Chung JK, Kim EE & Lee DS (2015) Prognostic value of volumetric parameters of 18F-FDG PET in non-small-cell lung cancer: a meta-analysis. *Eur J Nucl Med Mol Imaging* **42**, 241–251.

85 Wever W, Ceyssens S, Mortelmans L, Stroobants S, Marchal G, Bogaert J & Verschakelen JA (2007) Additional value of PET-CT in the staging of lung cancer: comparison with CT alone, PET alone and visual correlation of PET and CT. *Eur Radiol* **17**, 23–32.

86 Kung B, Yong TA & Tong C (2017) The pearl of FDG PET/CT in preoperative assessment of patients with potentially operable non-small-cell lung cancer and its clinical impact. *World J Nucl Med* **16**, 21.

87 Effert PJ, Bares R, Handt S, Wolff JM, Büll U & Jakse G (1996) Metabolic imaging of untreated prostate cancer by positron emission tomography with 18fluorine-labeled deoxyglucose. *J Urol* **155**, 994–998.

88 Lawrentschuk N, Davis ID, Bolton DM & Scott AM (2006) Positron emission tomography and molecular imaging of the prostate: an update. *BJU Int* **97**, 923–931.

89 Bouchelouche K & Oehr P (2008) Positron emission tomography and positron emission tomography/computerized tomography of urological malignancies: an update review. *J Urol* **179**, 34–45.

90 Rohren EM, Turkington TG & Coleman RE (2004) Clinical applications of PET in oncology. *Radiology* **231**, 305–332.

91 Podo F (1999) Tumour phospholipid metabolism. *NMR Biomed* **12**, 413–439.

92 De Jong IJ, Pruim J, Elsinga PH, Vaalburg W & Mensink HJ (2003) Preoperative staging of pelvic lymph nodes in prostate cancer by 11C-cholme PET. *J Nucl Med* **44**, 331–335.

93 Sutinen E, Nurmi M, Roivainen A, Varpula M, Tolvanen T, Lehikoinen P & Minn H (2004) Kinetics of [11C]choline uptake in prostate cancer: a PET study. *Eur J Nucl Med Mol Imaging* **31**, 317–324.

94 Welle CL, Cullen EL, Peller PJ, Lowe VJ, Murphy RC, Johnson GB & Binkovitz LA (2016) C-choline PET/CT in recurrent prostate cancer and nonprostatic neoplastic processes. *Radiographics* **36**, 279–292.

95 Mesguich C, Hulin C, Lascaux A, Bordenave L, Marit G & Hindié E (2020) Choline PET/CT in multiple myeloma. *Cancers (Basel)* **12**, 1394.

96 Talbot JN, Gutman F, Fartoux L, Grange JD, Ganne N, Kerrou K, Grahek D, Montravers F, Poupon R & Rosmorduc O (2006) PET/CT in patients with hepatocellular carcinoma using [18F]fluorocholine: preliminary comparison with [18F]FDG PET/CT. *Eur J Nucl Med Mol Imaging* **33**, 1285–1289.

97 Andriole GL, Kostakoglu L, Chau A, Duan F, Mahmood U, Mankoff DA, Schuster DM, Siegel BA, Adler LP, Belkoff LH et al. (2019) The impact of positron emission tomography with 18 F-fluciclovine on the treatment of biochemical recurrence of prostate cancer: results from the LOCATE trial. *J Urol* **201**, 322–331.

98 Schülke N, Varlamova OA, Donovan GP, Ma D, Gardner JP, Morrissey DM, Arrigale RR, Zhan C, Chodera AJ, Surowitz KG et al. (2003) The homodimer of prostate-specific membrane antigen is a functional target for cancer therapy. *Proc Natl Acad Sci USA* **100**, 12590–12595.

99 O'Keefe DS, Bacich DJ, Huang SS & Heston WDW (2018) A perspective on the evolving story of PSMA biology, PSMA-based imaging, and endoradiotherapeutic strategies. *J Nucl Med* **59**, 1007–1013.

100 Maurer T, Gschwend JE, Rauscher I, Souvatzoglou M, Haller B, Weirich G, Wester HJ, Heck M, Kübler H, Beer AJ et al. (2016) Diagnostic efficacy of 68Gallium-PSMA positron emission tomography compared to conventional imaging for lymph node staging of 130 consecutive patients with intermediate to high risk prostate cancer. *J Urol* **195**, 1436–1443.

101 Thomas L, Balmus C, Ahmadzadehfar H, Essler M, Strunk H & Bundschuh RA (2017) Assessment of bone metastases in patients with prostate cancer—a comparison between 99mTC-bone-scintigraphy and [68Ga]Ga-PSMA PET/CT. *Pharmaceuticals* **10**, 1–9.

102 Eiber M, Maurer T, Souvatzoglou M, Beer AJ, Ruffani A, Haller B, Graner FP, Kübler H, Haberhorn U, Eisenhut M et al. (2015) Evaluation of hybrid 68Ga-PSMA ligand PET/CT in 248 patients with biochemical recurrence after radical prostatectomy. *J Nucl Med* **56**, 668–674.

103 Alipour R, Azad A & Hofman MS (2019) Guiding management of therapy in prostate cancer: time to switch from conventional imaging to PSMA PET? *Ther Adv Med Oncol* **11**, 1–14.

104 Ardenkjaer-Larsen JH, Fridlund B, Gram A, Hansson G, Hansson L, Lerche MH, Servin R, Thaning M & Golman K (2003) Increase in signal-to-noise ratio of >10,000 times in liquid-state NMR. *Proc Natl Acad Sci USA* **100**, 10158–10163.

105 Nelson SJ, Kurhanewicz J, Vigneron DB, Larson PEZ, Harzstark AL, Ferrone M, van Criekinge M, Chang JW, Bok R, Park I et al. (2013) Metabolic imaging of patients with prostate cancer using hyperpolarized [1-13C] Pyruvate. *Sci Transl Med* **5**, 198ra108.

106 Marco-Rius I, Tayler MCD, Kettunen MI, Larkin TJ, Timm KN, Serrao EM, Rodrigues TB, Pileio G, Ardenkjaer-Larsen JH, Levitt MH et al. (2013) Hyperpolarized singlet lifetimes of pyruvate in human blood and in the mouse. *NMR Biomed* **26**, 1696–1704.

107 Chen HY, Gordon JW, Bok RA, Cao P, von Morze C, van Criekinge M, Milshteyn E, Carvajal L, Hurd RE, Kurhanewicz J et al. (2019) Pulse sequence considerations for quantification of pyruvate-to-lactate conversion kPL in hyperpolarized 13C imaging. *NMR Biomed* **32**, 1–14.

108 Keshari KR & Wilson DM (2014) Chemistry and biochemistry of 13C hyperpolarized magnetic resonance using dynamic nuclear polarization. *Chem Soc Rev* **43**, 1627–1659. https://doi.org/10.1039/c3cs60124b

109 Gallagher FA, Kettunen MI, Hu D-E, Jensen PR, Zandt RIT, Karlsson M, Gisselsson A, Nelson SK, Witney TH, Bohndiek SE et al. (2009) Production of hyperpolarized [1,4–13C2]malate from [1,4–13C2]fumarate is a marker of cell necrosis and treatment response in tumors. *Proc Natl Acad Sci USA* **106**, 19801–19806.

110 von Morze C, Larson PEZ, Hu S, Keshari K, Wilson DM, Ardenkjaer-Larsen JH, Goga A, Bok R, Kurhanewicz J & Vigneron DB (2011) Imaging of blood flow using hyperpolarized [13C]Urea in preclinical cancer models. *J Magn Reson Imaging* **33**, 692–697.

111 Gallagher FA, Kettunen MI, Day SE, Hu D-E, Ardenkjær-Larsen JH, Zandt R, Jensen PR, Karlsson M, Golman K, Lerche MH *et al.* (2008) Magnetic resonance imaging of pH *in vivo* using hyperpolarized 13C-labelled bicarbonate. *Nature* **453**, 940–943.

112 Granlund KL, Tee SS, Vargas HA, Lyashchenko SK, Reznik E, Fine S, Laudone V, Eastham JA, Touijer KA, Reuter VE *et al.* (2020) Hyperpolarized MRI of human prostate cancer reveals increased lactate with tumor grade driven by monocarboxylate transporter 1. *Cell Metab* **31**, 105–114.e3.

113 Aggarwal R, Vigneron DB & Kurhanewicz J (2017) Hyperpolarized 1-[13C]-pyruvate magnetic resonance imaging detects an early metabolic response to androgen ablation therapy in prostate cancer. *Eur Urol* **72**, 1028–1029.

114 Tessem MB, Swanson MG, Keshari KR, Albers MJ, Joun D, Tabatabai ZL, Simko JP, Shinohara K, Nelson SJ, Vigneron DB *et al.* (2008) Evaluation of lactate and alanine as metabolic biomarkers of prostate cancer using 1H HR-MAS spectroscopy of biopsy tissues. *Magn Reson Med* **60**, 510–516.

115 Harris T, Eliyahu G, Frydman L & Degani H (2009) Kinetics of hyperpolarized 13C1-pyruvate transport and metabolism in living human breast cancer cells. *Proc Natl Acad Sci USA* **106**, 18131–18136.

116 Keshari KR, Sriram R, Koelsch BL, Van Criekinge M, Wilson DM, Kurhanewicz J & Wang ZJ (2013) Hyperpolarized 13C-pyruvate magnetic resonance reveals rapid lactate export in metastatic renal cell carcinomas. *Cancer Res* **73**, 529–538.

117 Chen HY, Larson PEZ, Bok RA, von Morze C, Sriram R, Delos Santos R, Delos Santos J, Gordon JW, Bahrami N, Ferrone M *et al.* (2017) Assessing prostate cancer aggressiveness with hyperpolarized dual-agent 3D dynamic imaging of metabolism and perfusion. *Cancer Res* **77**, 3207–3216.

118 Ardenkjaer-Larsen JH (2019) Hyperpolarized MR – what's up Doc? *J Magn Reson* **306**, 124–127.

119 Ardenkjaer-Larsen JH (2016) On the present and future of dissolution-DNP. *J Magn Reson* **264**, 3–12.

120 Nishino M, Jagannathan JP, Ramaiya NH & Van Den Abbeele AD (2010) Revised RECIST guideline version 1.1: what oncologists want to know and what radiologists need to know. *Am J Roentgenol* **195**, 281–289.

121 Taylor FGM, Quirke P, Heald RJ, Moran BJ, Blomqvist L, Swift IR, Sebag-Montefiore D, Tekkis P & Brown G (2014) Preoperative magnetic resonance imaging assessment of circumferential resection margin predicts disease-free survival and local recurrence: 5-Year follow-up results of the MERCURY Study. *J Clin Oncol* **32**, 34–43.

122 Padhani AR, Liu G, Mu-Koh D, Chenevert TL, Thoeny HC, Takahara T, Dzik-Jurasz A, Ross BD, Van Cauteren M, Collins D *et al.* (2009) Diffusion-weighted magnetic resonance imaging as a cancer biomarker: consensus and recommendations. *Neoplasia* **11**, 102–125.

123 Mann RM, Kuhl CK, Kinkel K & Boetes C (2008) Breast MRI: guidelines from the European Society of Breast Imaging. *Eur Radiol* **18**, 1307–1318.

124 Kurhanewicz J, Vigneron DB, Ardenkjaer-Larsen JH, Bankson JA, Brindle K, Cunningham CH, Gallagher FA, Keshari KR, Kjaer A, Laustsen C *et al.* (2019) Hyperpolarized 13C MRI: path to clinical translation in oncology. *Neoplasia (United States)* **21**, 1–16.